Biomedicine & Pharmacotherapy 156 (2022) 113909

Contents lists available at ScienceDirect

Biomedicine & Pharmacotherapy

journal homepage: www.elsevier.com/locate/biopha

New local ganirelix sustained release therapy for uterine leiomyoma. Evaluation in a preclinical organ model

Ana Salas [a,b,1], Patricia García-García [c,d,1], Patricia Díaz-Rodríguez [d,e], Carmen Évora [c,d], Teresa A. Almeida [a,b,*], Araceli Delgado [c,d,**]

[a] Department of Biochemistry, Microbiology, Cell Biology and Genetics, Universidad de La Laguna, 38206 La Laguna, Spain
[b] Instituto Universitario de Enfermedades Tropicales y Salud Pública de Canarias, 38206 La Laguna, Spain
[c] Department of Chemical Engineering and Pharmaceutical Technology, Universidad de La Laguna, 38206 La Laguna, Spain
[d] Institute of Biomedical Technologies (ITB), Universidad de La Laguna, 38206 La Laguna, Spain
[e] Department of Pharmacology, Pharmacy and Pharmaceutical Technology, I+D Farma Group (GI-1645), Facultad de Farmacia, Instituto de Materiales (iMATUS) and Health Research Institute of Santiago de Compostela (IDIS), Universidade de Santiago de Compostela, 15782 Santiago de Compostela, España

ARTICLE INFO

Keywords:
Gonadotropin-releasing hormone (GnRH) antagonists
Leiomyoma
Ganirelix
PLGA-microspheres
Local delivery
Preclinical model

ABSTRACT

Currently, there is a limited number of treatment options available for patients with symptomatic leiomyomas, and surgical removal is by far the most frequent procedure. Previous studies found that GnRH agonists and antagonists acting through GnRH receptors led to cell death and decreased extracellular synthesis in cultured leiomyoma cells. In this study, we encapsulated the GnRH antagonist ganirelix in PLGA microspheres contained in an alginate scaffold that also supports a leiomyoma *ex vivo* tissue explant. Microspheres maintained ganirelix concentration stably during six days of culture, inducing significant cell death in 50–55% of tumor cells. Although no changes were observed in the expression of extracellular matrix genes, a decreased expression of the Nuclear Factor of Activated T cells 5, a transcription factor involved in osmotic stress and tumor size. Interestingly, all tumors analyzed experienced apoptosis independently of the original driver mutation. These data indicate that local therapy of ganirelix would induce tumor reduction in a wide range of uterine leiomyomas.

1. Introduction

Uterine leiomyomas (LMs), also called fibroids or myomas, are the most commonly diagnosed tumor of the female genital tract, with an incidence of 40% at the age of 35 and nearly 70%– 80% around the age of 50 [1]. This high prevalence represents a high economic burden to the global healthcare costs estimated to be 34.4 billion dollars just in the United States [2]. Although these tumors are benign, 15–30% of patients develop several symptoms, with menorrhagia or heavy menstrual bleeding being the most common ones [1]. Other LM symptoms include abdominal protuberance, painful intercourse, pelvic pressure, bladder or bowel dysfunction resulting in urinary incontinence or retention, pain, or constipation [3]. In addition, LM may interfere with natural and *in vitro* fertility and increase the risk of adverse pregnancy outcomes [3]. Surgical options are by far the most frequent treatment for LM [4].

Although their etiology remains elusive, molecular mechanisms involved in tumor initiation and growth include steroid hormone-dependency, excessive accumulation of extracellular matrix (ECM) and alterations in two driver genes, *HMGA2* (high mobility group AT-hook 2) and *MED12* (mediator complex subunit 12), found in approximately 80–90% of leiomyomas [5].

Current pharmacological approaches are based on the pivotal role of ovarian steroids in LM growth [6]. In normal conditions, the hypothalamus exerts control over sex steroid production *via* GnRH, which induces the release of pituitary gonadotropins, stimulating the production of estrogen and progesterone in the ovary [6]. The GnRH antagonists binding to the GnRH receptor (GNRHR) cause an immediate dose-dependent suppression of gonadotropin release [7]. This sex steroid inhibition significantly decreases LM volume in pre-menopausal women while abolishing menorrhagia symptoms and reducing uterine pain [8]. Unfortunately, the use of GnRH antagonists (GnRHa) to decrease ovarian steroids has traditionally been associated to substantial

* Corresponding author at: Department of Biochemistry, Microbiology, Cell Biology and Genetics. Universidad de La Laguna, 38206 La Laguna, Spain.
** Corresponding author at: Department of Chemical Engineering and Pharmaceutical Tecnology, Universidad de La Laguna, 38206 La Laguna, Spain.
E-mail addresses: tacosalm@ull.edu.es (T.A. Almeida), adelgado@ull.edu.es (A. Delgado).
[1] These authors have contributed equally to this work

https://doi.org/10.1016/j.biopha.2022.113909
Received 7 July 2022; Received in revised form 17 October 2022; Accepted 19 October 2022
Available online 21 October 2022

side effects, including vasomotor symptoms, vaginal dryness, sleep disturbances, myalgia, arthralgia, mood swings, potential cognitive impairment, and loss in bone density impairing long-term treatments [8]. Nevertheless, the emergence of new GnRHa for oral administration, such as relugolix, recently approved by the EMA and FDA, linzagolix approved by EMA, and elagolix approved by FDA has allowed for more prolonged LMs treatments reaching up to 24 months. However, despite reducing menstrual bleeding and tumor volume, these novel treatment options do not lack detrimental systemic effects. Indeed, relugolix and elagolix are co-administered with estradiol and norethisterone as an "add-back" therapy to avoid undesirable hypoestrogenic effects such as reduced bone mineral density [9,10].

Although it has always been thought that LMs shrinkage after GnRHa treatment was attributable to a decreased sex steroid release, a growing body of evidence suggests a direct GnRH action on peripheral tissues [11–13]. Thus, leiomyomas, myometrium, and isolated myometrial smooth muscle cells express GnRH and the GnRH receptor at the mRNA and protein levels [14–19]. The GnRH antagonist cetrorelix acetate inhibited leiomyoma cell growth, induced apoptosis, and decreased the production of ECM components in LM cells in culture [20,21]. However, since traditional 2D cultures where cells grow in flat layers on plastic surfaces do not accurately mimic the *in vivo* state, some caution should be applied to these results. This is quite relevant since many drugs proving to be clinically futile were pre-clinically evaluated to be 'active' using 2D-cultured cell line-based models [22]. Cetrorelix acetate also inhibited ECM production in a 3D matrix using immortalized leiomyoma cell lines. This effect was not suppressed in the presence of gonadal hormones [23]. All these data suggest a direct action of GnRH antagonist on LM cells.

Ganirelix is a third-generation GnRHa that inhibits premature LH surges in women undergoing controlled ovarian hyperstimulation for assisted reproductive technologies. Ganirelix displays a long half-life of approximately 12.8 h [24] and for the above purpose is administered in solution (at 0.25 mg/day) subcutaneously, usually for 5–6 days. Interestingly, a small, open-label study including 19 patients with LM demonstrated the daily subcutaneous treatment with 2 mg ganirelix substantially reduced LM volume (25–40%) within only three weeks [25].

Considering the readily accessible route for drug delivery through the vagina [26], the lack of local treatments for the management of LM, and the side effects associated with GnRHa systemic administration, it is surprising that formulations for local GnRHa administration are still not available.

In our previous study, we developed an organotypic 3D culture based on leiomyoma tissue explants placed onto an alginate scaffold. This approach successfully maintained the original LM cells, tumor microenvironment, and the response of cells to ovarian steroids [27]. As a step forward in developing a local therapy for uterine leiomyoma, the main goal of the current study is to evaluate the effect of sustained release of ganirelix on LM explants. We measured cell death using the TUNEL assay and genes affecting LM size, such as those involved in the ECM and cell water balance. This preclinical assay will highlight the microspheres as potential GnRHa carriers for leiomyoma local therapy.

2. Materials and methods

2.1. Ethical statement

This study was approved by the Institutional Review Board of the Committee for Clinical Research Ethics of the University Hospital Complex from Canary Island (CHUNSC_2018_63). Informed consent was obtained from the patients before the collection of any samples. All experiments handling human tissues were performed in accordance with Tenets of the Declaration of Helsinki.

2.2. Systems preparation and characterization

2.2.1. Materials

Poly (lactic-co-glycolic acid) (PLGA) of variable lactic:glycolic ratios, 75:25 (PLGA 75:25, Resomer® RG 755 S) and 85:15 (PLGA 85:15, Resomer® RG 858 S) were purchased from Evonik Industries (Germany). Sodium alginate (Protasan® UP MVG) was obtained from Novamatrix (Biopolymer Systems, Norway). Poly (vinyl alcohol) (PVA, Mw 33,000–70,000; 87–90% hydrolyzation), Span 60 (Sorbitane monostearate, Mw: 430.63 g/mol, HLB: 4.7) and ganirelix acetate salt (Mw: 1690.42 g/mol) were supplied by Sigma-Aldrich (USA). Calcium Chloride ($CaCl_2$) and Sodium Chloride (NaCl) were purchased from Merck (Germany).

2.2.2. Ganirelix microspheres preparation

Ganirelix microspheres were prepared by a double emulsion method (w/o/w) similarly to previously described [28]. Two types of microspheres were developed, one of them containing 2% of sodium alginate in the internal aqueous phase (AlgMPs-G) [29,30], and another one without (MPs-G). Briefly, 200 μl of an aqueous solution containing 75 μg of ganirelix acetate salt and 4 mg of sodium alginate, when required, was emulsified with 1.5 mL of a PLGA (200 mg of PLGA 75:25, 50 mg of PLGA 85:15 and 0.3 mg of Span 60) [31] methylene chloride (DCM) solution vortexed for 1 min. Immediately, 5 mL of a 5% poly-vinyl alcohol (PVA) and 5% NaCl aqueous solution was added and vortexed for 30 s. Afterward, the emulsion was poured in 100 mL of water under magnetic stirring to evaporate the solvent for 1.5 h. Microspheres were collected by filtration (Supor®−450, 0.45 μm, 47 mm filters, Pall Corporation) and washed with Milli-Q water. Then, microspheres were lyophilized and stored at 4 °C until use. Blank microspheres, without ganirelix, were prepared by the same method.

Microspheres were characterized in terms of diameter and size distribution using a Mastersizer 2000 (Malvern Instruments, USA), and morphology was observed by scanning electron microscopy images (SEM, ZEISS EVO 15, Japan).

To assess the encapsulation efficiency and release profile, ganirelix was labelled with ^{125}I (Perkin-Elmer) by the iodogen method according to the protocol previously described [32] with some modifications. Briefly, 50 μl of phosphate buffer (PB: 0.5 M) and 20 μl of ganirelix acetate (10 μg/μl, 5.9×10^{-3} M) were added to a precoated Iodination Tube (Thermo Scientific), and the sample volume was completed with Milli-Q water to obtain a final volume of 98 μl. Then, 2 μl of ^{125}INa (0.2 mCi) (PerkinElmer) were added to the previous mixture. This reaction mixture was incubated for 10 min at room temperature under 120 rpm stirring and stopped by addition of 10 μl sodium metabisulphite (2.5 mg/mL). The labeling efficiency was evaluated by thin layer chromatography (iTLC) using 11.5 × 0.8 cm silica-gel coated strips (Varian Iberica SL). For that purpose, 7 μl of ^{125}I-ganirelix (approximately 30, 000–40,000 cpm) were added approximately at 1 cm from the lower edge of the strip and the chromatography was developed using methanol:water (85:15) as a mobile phase [33]. Free ^{125}I migrates to the front (R_f=1) and the labeled product continues at the base (R_f=0). When the solvent reached the front (approximately 1 cm from the upper edge), the strip was cut by the half, and the radioactivity of each measured using a gamma counter (Cobra II, Packard®). The labeling yield was calculated by the ratio between the radioactivity at the base (Rf=0) and the total radioactivity (Rf=0 + Rf=1) x 100. The same method was used to study the radiolabeling stability. Briefly, 2 μl of ^{125}I-ganirelix were incubated in 250 μl of Dulbecco's phosphate-buffered saline (dPBS) at 4 °C and 37 °C under 25 rpm stirring. Then, at different time points (0, 0.6, 3 and 4 days), the chromatography of a sample was made to calculate the ^{125}I unbound. Assays were performed in triplicate.

2.3. Scaffold preparation and characterization

Scaffolds were prepared as previously described [27]. Briefly, 2 mg

of microspheres were dispersed in 100 μl of 2% sodium alginate aqueous solution in a cylindrical mould, mixed and freeze-dried. Then, alginate was crosslinked with 100 μl of 1% $CaCl_2$ for 3 min, washed twice with 100 μl of sterile Milli-Q water, and freeze-dried again. All systems were stored at 4 °C until use. The scaffolds were characterized in terms of porosity, morphology (SEM), swelling and mass loss in water at 37 °C. Porosity was calculated using the following equation (Eq. A.1).

$$Porosity(\%) = \left(\frac{\rho\ real - \rho\ app}{\rho\ real}\right)100 \quad (A.1)$$

Where ρ_{real} and ρ_{app} are the real and the apparent scaffold density, respectively.

The real density was quantified using a helium pycnometer (AccuPyc 1330, Micromeritics, USA), and the apparent density was calculated from measure of weight and the volume of the samples (Eq. A.2)

$$Apparent\ density = \frac{weight}{\pi r^2 h} \quad (A2)$$

To calculate the scaffolds swelling and mass loss, samples were incubated in 1 mL of Milli-Q water at 37 °C under orbital shaking (25 rpm). At different time points (1, 3 and 6 days), three samples were withdrawn, the excess water was removed, and samples were weighted and freeze-dried to record the dry weight. Scaffold swelling and mass loss were calculated by the following equations (Eq. A.3 and Eq. A.4 respectively).

$$Swelling = \left(\frac{W_w - W_i}{Ww}\right)100 \quad (A3)$$

$$Mass\ loss\left(\frac{W_o - W_d}{W_o}\right)100 \quad (A4)$$

Where W_w is sample wet weight, W_0 is initial weight, and W_d is dried weight.

2.4. Ganirelix release assay

Scaffolds developed with AlgMPs-^{125}I-G (S-AlgMPs-^{125}I-G) or with MPs-^{125}I-G (S-MPs-^{125}I-G) were incubated in 1.5 mL of DMEM (Dulbecco's modified Eagle's medium, Gibco) without supplements at 37 °C and 25 rpm. The supernatants were removed and replaced by fresh media at each time point. Then, the supernatant was measured with a gamma counter (Cobra® II, Packard). The experiment was performed in triplicate.

2.5. Tissue sampling

Six female patients aged 39–49 years, admitted to Hospital QuirónSalud in 2021, were enrolled in this study. All patients were Caucasian and underwent hysterectomy for menorrhagia without any previous hormonal treatment for at least 3 months before the surgery. One intramural leiomyoma up to 5–10 cm in size was obtained from each patient (Supplementary table S1). The histopathological analysis using standard H&E staining and performed by a pathologist indicated tumors with benign histology with no sign of malignancy, nuclear atypia, mitotic or necrosis. Samples were transported immediately after surgery immersed in sterile Hank's balanced salt solution (HBSS) supplemented with 0.25 μg/mL amphotericin B, 100 U/mL penicillin, and 100 μg/mL streptomycin (Sigma-Aldrich). Tissue pieces were then processed under sterile conditions.

2.6. Tissue slice culture

Fresh tissue sections of 500 μm were obtained using a vibratome and cultured as previously described [27]. Tissue slices were placed on 0.8 mm thickness alginate scaffolds containing blank microspheres in 24-well plates containing 250 μl of DMEM supplemented with 10% fetal bovine serum (FBS, Lonza, Spain), 100 U/mL penicillin, 100 μg/mL streptomycin and 2 mM L-Glutamine (Sigma-Aldrich) during 24 h to adapt the tissue cells to the culture conditions as described in Supplementary Figure 1. Slices were cultivated at the air-liquid interface in a 37 °C and 5% CO_2 humidified incubator with shaking at 60 rpm. The medium was changed every day. After the initial 24 h, slices were transferred onto scaffolds containing ganirelix-microspheres (S-AlgMPs-G and S-MPs-G groups) or remained on the original blank-microspheres scaffolds with the medium supplemented every day with 10^{-8} M ganirelix solution (S-G group) or not supplemented (Control group) for 6 days (Supplementary Figure 1). We have previously tested 3 concentrations of ganirelix (10^{-7}, 10^{-8} and 10^{-9} M) during 3 different times (2, 4 and 6 days), and we found that a 10^{-8} M ganirelix supplementation during 6 days led to greater apoptosis in tumor cells in the *ex vivo* slices. Working dilutions were prepared in phenol red-free DMEM medium every day immediately at the start of the experiment. A droplet of the medium was added on top of the tissue slice to create a thin film of liquid that helps to maintain the explant humidity [34]. In supplemented group, the droplet contains ganirelix solution. For each tumor, 2 slices were harvested before culture (T0), one of them was kept at − 80 °C until processed for molecular analysis, while the other was formalin-fixed for histological analysis. Another 5 slices were collected after 6 day of treatment, 2 slices were formalin-fixed, and 3 slices were frozen at − 80 °C for molecular analysis.

2.7. Genetic alterations. characterization of driver genes

2.7.1. Nucleic acid isolation and reverse transcription

Tissue slices were placed on lysis matrix D tubes (MP Biomedicals) containing 500 μl of Tritidy G (PanReac AppliChem) and homogenized using FastPrep 5 G (2 cycles of 6 m/s for 30 s; MP Biomedicals). RNA was isolated following manufacturer instructions (PanReac AppliChem). Residual genomic DNA was removed by incubating the RNA samples with RNase-free DNase I and RNasin according to the manufacturer's instructions (Promega). Retro-transcription was carried out using 1 μg of RNA, and first-strand complementary DNA was synthesized using M-MLV reverse transcriptase according to the manufacturer's instructions (M3681, Promega).

2.7.2. HMGA2 expression

PCR mixes contained 0,25 pmol of each primer [27], 1 unit of TempTase DNA Polymerase (Thermofisher Scientific), 150 μM dNTPs and 4 μl of cDNA (1/12 dilution) in a final volume of 20 μl. The cycling conditions were 95 °C for 15 min, followed by 40 cycles of 95 °C for 15 s, 66 °C for 20 s, and 72 °C for 30 s. For each experiment, a non-sample reaction was included as a negative control. The PCR products were separated by agarose gel electrophoresis, and the amplicon size was verified by comparison with a 100-bp DNA ladder.

2.7.3. MED12 mutation detection

To check for MED12 mutations in cDNA, a primer pair located in exon 1 and exon 2 covering the hot spot region where 99% of mutations have been described was used [27]. PCR products were cleaned up by ExoSAP treatment using ExoCleanUp FAST (VWR Life Science). Sequencing reactions were performed for both strands at the Genomic Center of La Laguna University (SEGAI). For each sample, forward and reverse electropherograms were checked manually, edited, and assembled using MEGA6 [35].

2.8. Quantitative polymerase chain reaction (qPCR)

A Light-Cycler 480 Real-Time PCR detection system apparatus was used to quantify of all transcripts. Each sample was analyzed in triplicate using 2x qPCRBIO SyGreen Mix Lo-Rox (PCRBiosystems, London, UK). The cycling conditions were 95 °C for 2 min, followed by 35–40 cycles of 95 °C for 10 s, 60 °C for 20 s, and 72 °C for 30 s. For each experiment,

a non-template reaction was included as a negative control. The specificity of the PCR reactions was confirmed by melting curves analysis of the products.

Plates data were imported into the GenEx ver 6.1.1.550 data analysis software (MultiD Analyses AB). The relative expression of each gene was calculated using the $2^{-\Delta\Delta Ct}$ method normalized to the expression levels of two housekeeping genes (RPL32 and PUM1) stably expressed [36] and then referenced to the mean of controls (vehicle). Log2 transformation of fold-change was used for statistical analysis. Primer sequences are provided in Supplementary Table S2.

2.9. Histological evaluation

Before fixation in 10% buffered formalin, the air side of the slice was marked with green Ink for biopsies to evaluate changes between both sides of the slice. After fixation and paraffin-embedded, vertical sections were cut into 5 μm-thick sections. The sections were deparaffinated, hydrated and hematoxylin-eosin (H&E) stained to assess the morphological integrity of tissue samples.

To evaluate the amount of collagen in the original tumor, tissue sections were stained with Masson's trichrome following a standard protocol [37], which stains collagen fibbers blue. Briefly, after deparaffinization and rehydration, sections were post-fixed with Bouin's solution overnight. The slices were then rinsed in running tap water for 5 min and stained in Weigert's iron hematoxylin working solution for 10 min. Sections were counter-stained in Bierbrich scarlet-acid fuchsin solution for 2 min, rinsed in distilled water, and placed in the phosphomolybdic-phosphotungstic acid solution for 2 min. Subsequently, the sections were transferred to aniline blue solution for 5 min, rinsed in distilled water, and differentiated in 1% acetic acid solution for 4 min.

Image J Software version 1.5a (NIH) was used to quantify the collagen volume fraction. First, the total image area was measured, excluding white areas (vessels lumen and broken parts of the tissue). Second, the collagen volume was defined by selecting the blue staining area performing colour threshold and selecting hue, saturation, and brightness parameters. Finally, the tissue collagen volume fraction was determined using the following formula: collagen volume fraction = collagen area/total area × 100. Six fields were taken randomly under a light microscope (Leica DM4000B, Leica Microsystems, Germany) at a final magnification of X200. The final value was obtained by averaging the six fields.

2.10. Click-iT plus TUNEL assay

To determine the ganirelix effect at the tissue level, we performed a Click-It™ Plus TUNEL assay for *in situ* apoptosis detection following the manufacturer's instructions (C10617, Invitrogen). This assay detects the later stages of apoptosis when DNA fragmentation occurs. After labeling DNA ends with Alexa Fluor 488, the sections were incubated for 5 min with 1 μg/mL DAPI (Sigma-Aldrich) and mounted using Fluoromount-GTM mounting media (ThermoFisher Scientific). To assess apoptotic cells, six fields were randomly selected at a magnification of X400 under a fluorescence microscope (Leica DM4000B, Leica Microsystems, Germany), and two researchers blindly evaluated the images. Images obtained from different fluorescent channels were analyzed using the Image J program, version 1.5a software (NIH), where the program excluded stained fragments and artifacts after setting a threshold for minimum object size. Cells were considered positive when the fluorescent values were above the background of the non-dye reaction control. The apoptotic index (AI) was determined using the following formula: % apoptosis per field = positive apoptosis cells (Alexa 488 - green) / total cells (DAPI – blue) x 100. The final value was obtained by averaging the six fields.

2.11. Statistical analysis

GraphPad Prism v. 8.0 (GraphPad Software, La Jolla, CA, USA) was used for all statistical analyses. Original data were log-transformed, and the comparison among the groups was made by one-way ANOVA after assessing that the dataset passed the normality test, followed by Dunnett's *post hoc* test. For all analyses, $P < 0.05$ was considered to be statistically significant.

3. Results

3.1. System preparation and characterization

The dynamic light dispersion results showed that microspheres without alginate (MPs-G) were characterized by a lower average diameter (10% < 25.9 μm - 50% < 56.2 μm- 90% < 130.2 μm) than AlgMPs-G (10% < 26.8 μm - 50% < 85.7 μm- 90% < 173.2 μm). This increase in size was probably due to the presence of alginate in the internal aqueous phase.

SEM images indicated a similar external appearance for both types of microspheres (Fig. 1A-B), a homogeneous microspheres surface without external pores. The ganirelix encapsulation efficiency of MPs-G and AlgMPs-G was 55.09 ± 0.76% and 49.93 ± 5.91%, respectively.

A high radiolabeling yield of 90 ± 1% was obtained. These values were maintained after 4 days in dPBS without observing differences between 4 °C and 37 °C.

The SEM images of the alginate scaffolds showed a homogeneous dispersion of the microspheres within the internal scaffold structure (Fig. 1C). In agreement with these images, the scaffolds' porosity values were high, 95.65 ± 0.91%. Moreover, after the first 24 h, the scaffolds showed a large water uptake (305 ± 4.76%) with minimal mass loss (8.8 ± 0.5%). These values were maintained throughout the rest of the assay, indicating the stability of the structures.

3.2. Ganirelix released assay

The ganirelix release profile from S-AlgMPs-G showed a higher burst effect than S-MPs-G, with an initial release of 49.82 ± 8.11% from S-AlgMPs-G compared to 9.03 ± 1.04% from S-MPs-G (Fig. 2 A). The concentration of released ganirelix in the medium was 35.32×10^{-8} M for S-AlgMPs-G and 7.07×10^{-8} M for S-MPs-G during the first day. After that, the release rate decreased, and the concentration remained between 10 and 2×10^{-8} M for S-AlgMPs-G and 5–2×10^{-8} M for SMPs-G (Fig. 2B). Except for the burst effect of S-AlgMPs-G, the ganirelix concentration values obtained from both formulations remained of the same order of magnitude as the supplemented ganirelix in the medium (5×10^{-8} M).

3.3. Histological characterization of tumor cells after ganirelix treatment

The Innovative Medicines Initiative (IMI) consortium PREDECT (www.predect.eu) has established robust protocols to monitor cell viability status and to follow treatment responses in tumor tissue slice culture [38]. According to PREDECT, tumor slices embedded vertically can be sectioned to incorporate a scaffold to the air-side within one paraffin section, allowing analysis of both sides of the tissue slice. This is particularly important since H&E stained sections of vertically embedded tumor slices show differences in tissue morphology, presenting areas of necrosis, vacuolated regions, and reduced cells in the scaffold interface [38].

Similar to PREDECT findings, we observed decreased cell number and increased ECM and vacuolated cells in the region close to the alginate scaffold in all control samples, although at variable degrees. Fig. 3A shows a picture of a tumor slice with clear cell loss at the scaffold side. Therefore, to avoid an overestimation of apoptosis, we discarded from the analysis the 30 μm (Fig. 3A, dashed red line) of the slice in close

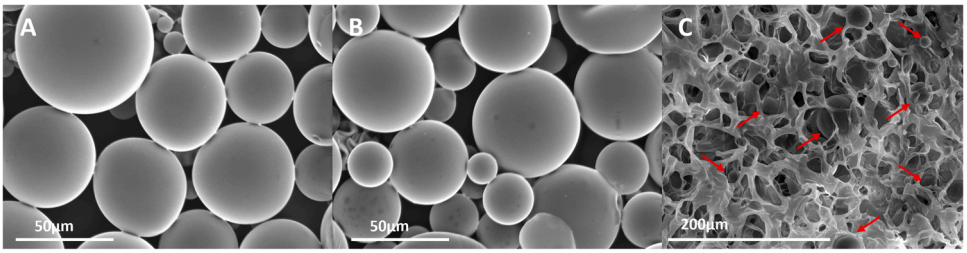

Fig. 1. Scanning electron microscopy images at 500X (A,B) and 300X (C). (A) Microspheres without alginate in the internal aqueous phase (MPs-G), (B) Microspheres with alginate in the internal aqueous phase (AlgMPs-G), and (C) Scaffold with microspheres (indicated with red arrows) dispersed in the alginate porous structure.

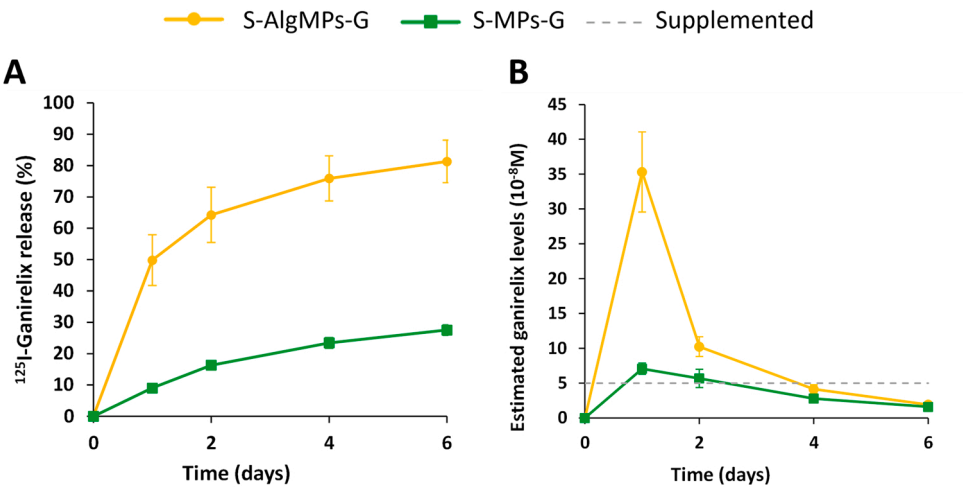

Fig. 2. ^{125}I-Ganirelix release profile in DMEM at 37 °C and 25 rpm, from the scaffolds containing microspheres with (S-AlgMPs-G) and without (S-MPs-G) alginate in the internal aqueous phase. The release profile is expressed in (A) ganirelix percentage released from the total loaded in the scaffold and (B) the calculated ganirelix molar concentration in the medium. The ganirelix level maintained by supplementation (5×10^{-8} M) is indicated for comparative purpose. N = 3.

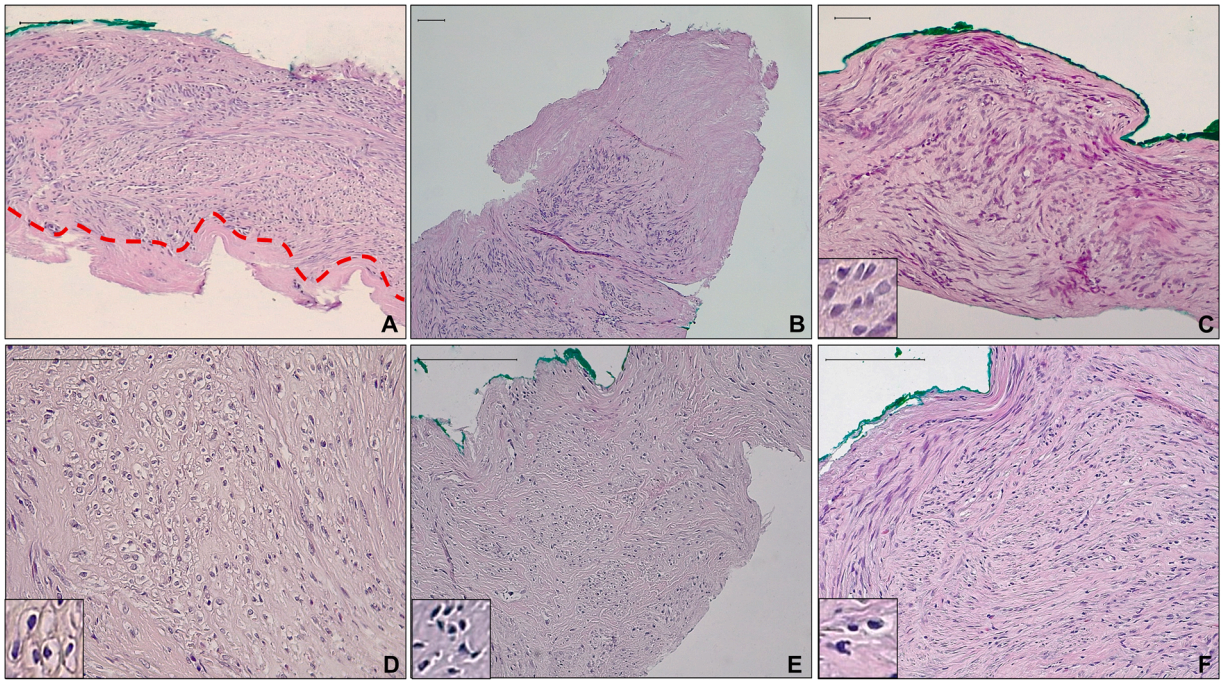

Fig. 3. Histological analysis of leiomyoma slices. Representative images of vertically embedded tumor tissue slices stained with H&E showing the increment of extracellular matrix in scaffold side (A) and the border of the tissue slice (B) compared with an area in the center of the slice (C). D-F shows morphological changes observed at 6 days after treatment with ganirelix supplemented in the medium (S-G) (D), or released from the microspheres in S-AlgMPs-G (E) and S-MPs-G (F), in comparison with the control slice (C). Asterisk denotes apoptotic nuclei, while arrowhead indicates vacuolated regions. Green Ink indicates slice air-side. The inserts (bottom left) show the morphology of the nucleus of the smooth muscle cells. Scale bar 100 µm.

contact with the scaffold. Similar to previously observed in tissue slices [39], the margins of the tissue sections showed a greater ECM content and variable degree of cell number (Fig. 3B). Thus, slice borders were also discarded from the analysis.

After ganirelix treatment, we observed cells with condensed, pyknotic nuclei and increased vacuolated cytoplasm indicating tissue degeneration (Fig. 3D-F). These findings were observed in the three experimental conditions, ganirelix supplemented in culture medium (Fig. 3D), ganirelix-PLGA-alginate microspheres (Fig. 3E) and ganirelix PLGA microspheres (Fig. 3F), but never in the untreated control (Fig. 3C).

3.4. TUNEL assay to identify apoptotic cells

Quantification of apoptotic cells can represent a critical aspect of toxicological assays and drug discovery. The TUNEL assay has become the most widely used *in situ* tests to study apoptosis [40]. More specifically, this assay detects the later stages of apoptosis, characterized by changes in nuclear morphology, chromatin condensation and DNA fragmentation. As expected, in the control slices cultured for 7 days, we detected DNA breaks preferentially on the scaffold side (Fig. 4B). In these untreated explants, the percentage of dead cells ranged from 10% to 28% (Supplementary Table S3) of the tissue area under study. Interestingly, a significant increase in the number of dead cells was observed

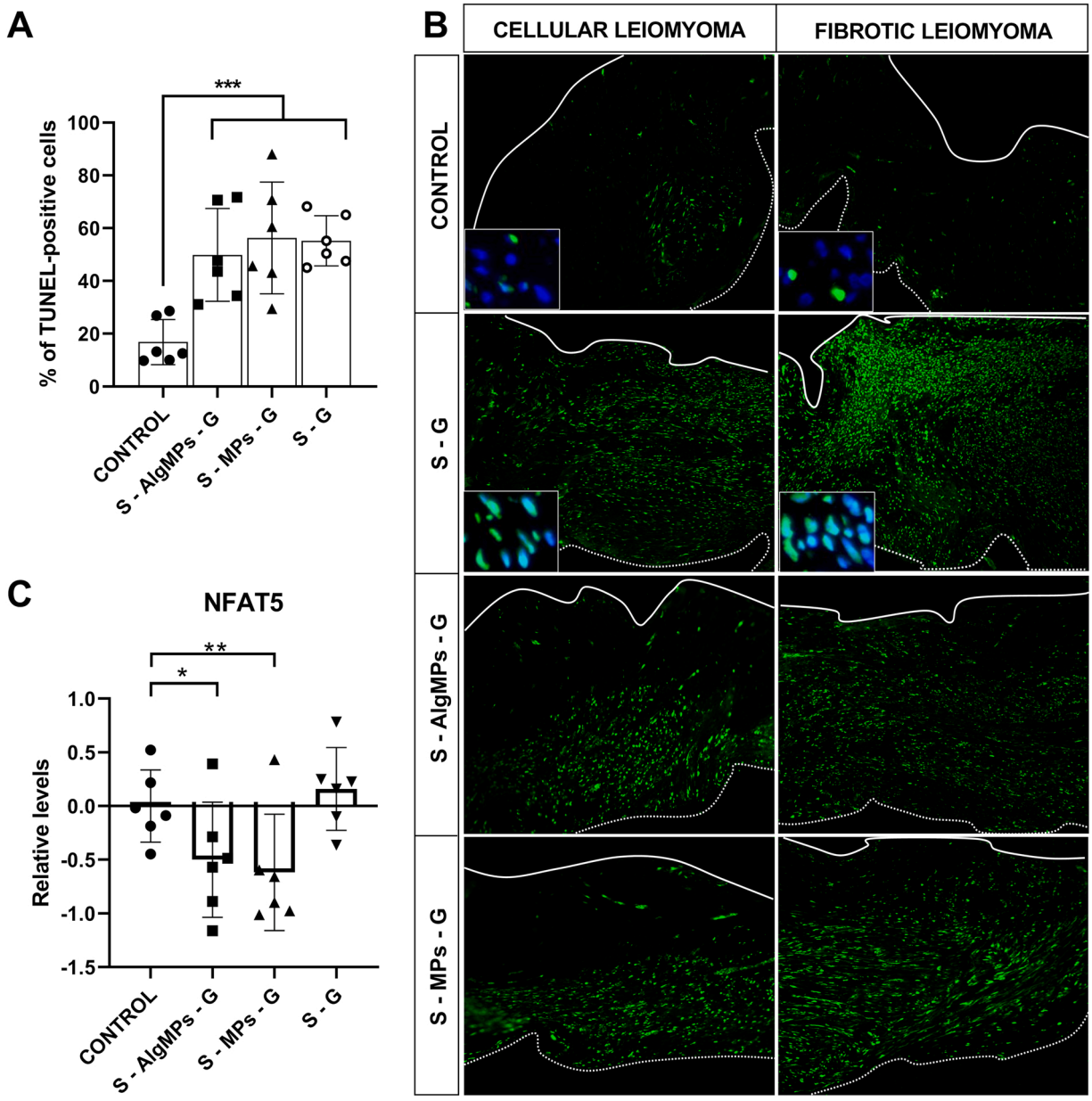

Fig. 4. Effect of ganirelix treatment in tumor slices. A) percentage of apoptotic cells in control (16.83 ± 8.6) and 3 experimental groups after 6 days of ganirelix exposure (S-G 55.2 ± 9.5; S-AlgMPs-G 48.9 ± 18.7; S-MPs-G 55.7 ± 22). Ganirelix significantly induced cell death in each treatment group compared to control slices (***$p < 0.001$). B) Panoramic images show apoptotic cell distribution across the slice in the cellular leiomyoma and a typical fibrotic tumor after Click-iT Plus TUNEL assay. DNA breaks were labelled with Alexa 488 (green), while DAPI was used to stain the nucleus (blue). The continuous line indicates the explant air side, while the dashed line indicates the explant scaffold side. Untreated tissue (control) showed few apoptotic cells compared with both ganirelix supplementation (S-G) and from both release systems, S-AlgMPs-G and S-MPs-G. Inserts indicate merge channels with the specific apoptotic reaction observed in the nuclei of the cells. Scale bar 100 μm. C) Relative expression of NFAT5 (nuclear factor of activated T cells 5) during ganirelix slice exposure compared with not treated (control) measured by qPCR. Bars show the mean fold change and error bars indicate standard deviation of the mean (SD). *$p < 0.05$. * *$p < 0.01$.

in tissue slices supplemented with ganirelix, or under continuous release from S-AlgMPs-G and S-MPs-G (Fig. 4A, $p < 0.001$). In addition, we observed a differential distribution of apoptotic cells throughout the slices depending on the amount of ECM. Masson's trichrome staining showed that leiomyoma L48 was a cellular tumor (Supplementary Figure 2), a rare leiomyoma variant that exhibits hypercellularity and occurs in < 5% of leiomyomas [41]. The remaining 5 tumors showed classical leiomyoma histology, with abundant fibrous matrix and variable collagen content (Supplementary Figure 1). Intriguingly, L48 showed the lowest percentage of dead cells in both release systems (Supplementary Table S3). Furthermore, we observed a gradient of apoptotic cells from the scaffold side towards the air-side in the cellular leiomyoma under the sustained release of ganirelix, but not in the supplemented slices, where the ganirelix solution reached the tissue slice from all the tumor sides (Fig. 4B). On the contrary, the apoptotic cells occupied practically the entire area analyzed in the fibrotic tumors.

Molecular analysis determined four LM subtypes according to driver alterations, one tumor carrying a *MED12* mutation, another tumor with overexpression of *HMGA2*, two tumors with both alterations and another two tumors without alterations in these two genes (Supplementary Table S1). It is worth mentioning that, regardless of their genetic alterations, all the tumors presented similar response to ganirelix treatment.

3.5. Effect of ganirelix on the expression of ECM genes and the osmoregulator NFAT5

ECM plays an important role in forming the bulk structure of leiomyoma, and its accumulation and remodelling are thought to be crucial in fibrotic diseases and their pathophysiology [8]. In order to determine the influence of ganirelix in ECM gene expression, we performed a qPCR of 3 genes highly expressed in leiomyomas. No statistically significant differences were observed on the expression of Collagen type I alpha 1 chain (COL1A1), the principal component of ECM, fibronectin 1 (FN1) and versican (VCAN) (Supplementary Figure 3). On the other hand, nuclear factor of activated T cells 5 (NFAT5) encode a protein that regulates gene expression induced by osmotic stress in mammalian cells. A significant downregulation of NFAT5 mRNA was detected after six days under 10^{-8} M ganirelix released from S-AlgMPs-G (1.41-fold, $p < 0.05$) and S-MPs-G (1.53-fold, $p < 0.01$) compared with untreated control (Fig. 4).

4. Discussion

Precision-cut tissue slices completely represent tumor architecture and heterogeneity, presenting the complex interplay between tumor and host cells in the stroma that plays a crucial role in tumor development, progression and response to therapy. Using the pre-clinical model developed by our group, we have proven the local effect of ganirelix in LMs, supporting a direct action of the GnRH antagonist on the tumor cells. These results open the possibility for leiomyoma management through GnRH antagonist local therapy avoiding the systemic side effects associated with oral administration.

Control slices may vary in the percentage of cell death during culture depending on *in vivo* basal cell death, complications in the operating room, tissue transportation times and duration of the processing. In addition, leiomyomas are quite heterogeneous tumors, with a variable number of cells and fibrous connective tissue, which lead to different tumor stiffness. Despite this, the percentage of dead cells after seven days of culture ranged from 10% to 28% in the tissue area under study, in agreement with previous reports in *ex vivo* cancer cultures, such as breast, pancreas, colon and lung carcinomas [42–44]. Interestingly, this initial cell death increased drastically after *ex vivo* incubation with ganirelix, both supplemented in the culture media or released from PLGA-microspheres. This pro-apoptotic effect was independent of the tumor driver mutation (Supplementary Table S1), indicating a wide range capacity of ganirelix for uterine leiomyoma treatment.

We have developed an innovative platform for culturing leiomyoma tissue onto a porous scaffold. The most significant novelty is that the scaffold contains drug-encapsulated microspheres that can be tested directly on the tumor tissue. We observed that ganirelix-microspheres did not decrease scaffold porosity (95.65%) while allowing an adequate supply of culture medium to tissue slices. In this platform, the scaffold presented a high swelling value and minimal mass loss, keeping the explants wet while ensuring system integrity. The treatment of the tumor tissue with ganirelix, induced a wide distribution of apoptotic cells, from the scaffold side to the air-side, using both microsphere formulations in five of the analyzed tumors, all of them showing abundant ECM. Conversely, in the cellular tumor, ganirelix released from microspheres resulted in a lower apoptosis rate than supplemented slices, with few dead cells observed towards the air-side of the slices. This is not surprising since tumors with high cell density and reduced interstitial space and ECM show lower drug penetration than tumors with a low packing density [45]. In this type of tumor, it is reasonable that the supplemented slices, with a greater diffusion surface due to the daily supply of ganirelix on top, presented a higher apoptosis rate (68%) than the tissue slices treated with ganirelix released from the microspheres (29–32%) where the surface available for drug diffusion is only the lower part in contact with the scaffold. However, other mechanisms may explain the reported differences in cell apoptosis.

The developed systems entail ganirelix doses well below the dose usually administered subcutaneously [24,46]. In addition, two different ganirelix releases were designed to study the effect of the release profile in cell apoptosis. Both PLGA microspheres incorporated into the alginate scaffold maintained ganirelix concentration in the 10^{-8} molar range. We hypothesized that adding alginate to the internal phase of the microsphere (S-AlgMPs-G) would modify the release profile [47]. Thus, the electrostatic interaction between the negative charges of the alginate and the positive charges of the peptide could reduce the release of ganirelix. However, the observed effect was not as expected, and the initial release of ganirelix was even higher than that from the microspheres without alginate (S-MPs-G). Alginate is a large molecule that could migrate towards the surface of the microspheres during the fabrication process, dragging ganirelix to the external surface. After the initial contact with the aqueous medium, ganirelix was abruptly released from the microspheres, giving the initial burst observed in the culture medium. Therefore, we took advantage of this release profile to compare the efficiency of a bolus dose followed by a continuous release with the sustained release profile observed with the S-MPs-G microspheres. Despite the differences in the release profiles, the apoptotic effect induced by both formulations was statistically equal to that observed with supplementation, indicating that drug concentrations in the range of $2–5 \times 10^{-8}$ M are indeed therapeutical and that an initial bolus does not improve the result. Considering the obtained release profiles, the use of microspheres without alginate is expected to be an effective and much safer formulation than S-AlgMPs-G, since it releases lower doses over a longer time. The initial ganirelix release from the alginate microspheres entails a higher risk of the drug reaching the bloodstream and producing similar undesirable effects to GnRHa systemic administration.

Extra-pituitary GNRHR has been found in several human cancers related to the reproductive system, such as prostate, breast, ovarian, and endometrial cancer [48]. Isolated LM smooth muscle cells express GnRH and GNRHR mRNA, while intense histological staining of GNRHR was observed in tumor smooth muscle cells [15,16,19]. In the central nervous system, GnRH agonists bind to GNRHR to stimulate Gαq and the production of inositol trisphosphate and diacylglycerol that consequently mobilize intracellular calcium and activate protein kinase C [49]. This drives the regulated exocytosis secretion of LH and FSH from secretory vesicles. The GnRH antagonists simply bind to pituitary GNRHR and competitively block the binding and activation by the native peptide in the gonadotrope cells. On the contrary, GnRH agonists

and antagonists in cancer cells seem to exert a similar effect, which is an intriguing open question. At the molecular level, several publications point to an equal and detrimental effect of GnRH agonists and antagonists on cancer cells [48]. For instance, GnRH agonists such as leuprolide, triptorelin, buserelin, and goserelin consistently inhibited, both *in vitro* and *in vivo*, the proliferation and the metastatic behavior of cell lines derived from tumors of the reproductive tract. In addition, GnRH agonists also exert a robust antitumor effect on cells derived from tumors unrelated to the hormonal system (melanoma, glioblastoma, and lung and pancreatic cancer), either *in vitro* or in preclinical models. Intriguingly, the most widely used GnRH antagonist *in vitro*, cetrorelix, showed antiproliferative activity in several studies: inhibiting the growth of androgen-independent prostate cancer cells, both *in vitro* and *in vivo*, and reducing the migratory and invasive behavior of DU145 prostate cancer cells; inhibiting the growth of prostate carcinoma primary cell cultures, an effect similar to that obtained with the GnRH agonist leuprolide; inhibiting the proliferation of human mammary estrogen-responsive tumor cells (MCF-7) *in vitro* and the growth of MCF-7 xenografts in nude mice; reducing metastasis formation by triple-negative MDA-MB-435 and MDA-MB-231 breast cancer cells in nude mice; exerting a similar antiproliferative activity as triptorelin in ovarian EFO-21 and endometrial HEC-1A cancer cells; in the OV-1063 ovarian cancer cell line, the antiproliferative activity of cetrorelix *in vitro* even exceeded that of the agonist triptorelin. In fibroids, cetrorelix inhibited leiomyoma cell growth, induced apoptosis, and decreased the production of ECM components in LM cells in culture. Similarly, buserelin inhibited cell proliferation in leiomyoma cells in a dose-dependent manner. Moreover, buserelin or leuprolide suppresses cell proliferation and induces apoptosis in human uterine leiomyoma cells. To explain these data, it has been proposed that binding of GnRH to GNRHR may activate different effectors in different cells [50]. Thus, in tumor cells, the binding of both GnRH agonist and antagonist to GNRHR induces Gαi/cAMP pathway, leading to antiproliferative and pro-apoptotic effects in reproductive tumors [48,51–53]. Although we have not analyzed the molecular mechanism involved in ganirelix signaling in leiomyoma cultures, the overwhelming data about the antiproliferative effect of agonist/antagonist in peripheral tumors strongly suggests a similar mechanism for both molecules in tumor cells.

Regarding leiomyomas, buserelin (a GnRH agonist) inhibited LM cell proliferation in a dose-dependent manner (ranging from 0 to 100 nM) after the 10th day of treatment [16]. Similarly, two GnRH agonists (leuprolide or buserelin) decreased cell number in a dose-dependent manner in isolated leiomyoma cells from premenopausal women, with the maximal effect observed at the highest dose tested (10^{-9} M) and after 6-day of treatment [17]. Moreover, using the TUNEL assay, the authors observed that GnRH agonist produced a significant increase in apoptotic cells after 4- and 6-day treatment while markedly increasing Fas and Fas ligand expression, suggesting activation of the extrinsic apoptotic pathway [17]. Chen et al. (2005) treated cultured leiomyoma cells with the antagonist cetrorelix acetate, observing a dose (10^{-6} M to 10^{-7} M) and time (2, 4, 6 days) dependent decrease of cell proliferation after 6 days of culture. In addition, cetrorelix (10^{-6} M to 10^{-7} M) also significantly increased TUNEL-positive cells after 36 h of treatment [20]. In light of these data, it is conceivable that ganirelix may bind to the GNRHR receptors widely expressed in leiomyoma smooth muscle cells, activating pathways that lead to apoptosis. This effect can be more pronounced in leiomyomas from reproductive women, where expression of the GnRH receptor is higher than in the myometrium, regardless of the myoma size [19]. Therefore, the local action of ganirelix controlled release in young women would be more specific and less damaging to the surrounding myometrium.

One distinguishing characteristic of uterine leiomyoma is the excessive accumulation of ECM, especially large amounts of disordered, highly cross-linked interstitial collagens, fibronectin, and proteoglycans, such as versican, an extracellular chondroitin sulfate proteoglycan known to be upregulated in leiomyoma tissue. The critical role of the ECM in the process of LM fibrosis turns it a crucial target for antifibrotic therapy. In this sense, the addition of GnRH agonist or antagonists (leuprolide acetate and cetrorelix) to leiomyoma cells during 24 and 72 h induced a deregulated expression of genes involved in ECM synthesis, including Collagen type I alpha 1 chain (COL1A), Fibronectin (FN), and Versican (VCAN) [19,21]. In this study, the treatment with 10^{-8} M of ganirelix in cultured LM slices for 6 days did not significantly change the mRNA expression of *COL1A1*, *FN*, and *VCAN*.

On the other hand, it has been hypothesized that the GnRH treatment causes water efflux from leiomyoma cells, resulting in a reduction in leiomyoma volume [54]. This mechanism seems to be mediated by NFAT5, a transcription factor involved in osmolytes accumulation to restore cellular homeostasis [55]. NFAT5 is upregulated in LM compared to myometrium [55,56]. Interestingly, either the GnRH agonist leuprolide [54] or a selective progesterone receptor modulator, Ulipristal Acetate [56], decreased the expression of *NFAT5* mRNA, suggesting that water outflow and cell shrinkage may explain the reduction in leiomyoma size after therapy [54,56]. In agreement with these studies, we also observed a decreased expression of *NFAT5* mRNA after ganirelix-controlled release treatment. Again, these data suggest that both types of drugs (agonist and antagonist) activate a common pathway in tumor cells. Exactly how ganirelix affects *NFAT5* expression and why *NFAT5* downregulation was observed only under ganirelix sustained release remains to be elucidated.

Overall, adding ganirelix to LM cells induced apoptosis and decreased the expression of *NFAT5*, suggesting the local therapy of ganirelix may reduce leiomyoma size.

The main strength of this *in vitro* study is the use of a 3D LM model to evaluate a novel local therapy for LM management. This tissue model preserves the extracellular matrix, cellular diversity, and genetic background, simulating more *in-vivo*-like situations. In addition, developing a formulation-dependent sustained ganirelix-release system opens the possibility of tailorable ganirelix doses. However, the study also has some limitations such as the inability to study the effect of ganirelix beyond 6 days due to limitations of the culture model; whether ganirelix promotes a reduction in ECM components at the protein level has not been tested; and finally, due to its low frequency, only one cellular LM has been studied.

Considering the promising pro-apoptotic effect observed on LM after treatment with sustained release, future works will evaluate the ganirelix effect over longer time periods and repeated administrations using *in vivo* models. Moreover, microspheres loaded with ganirelix can be embedded in intrauterine devices, favoring local administration. Controlled-drug release would favor a reduction in the overall tumor burden while minimizing systemic side effects.

5. Conclusions

The local release of ganirelix from the microspheres developed in this study induced cell death in leiomyoma organ culture. However, the cellular LM with a reduced matrix would need additional injections in different sites to achieve the same efficacy as in fibrotic tumors.

These results suggest that local treatment with ganirelix microspheres can potentially shrink leiomyomas and thereby relieve symptoms, and delay or even avoid surgery, since leiomyomas spontaneously regress at menopause due to the absence of ovarian steroids. In addition, it would also avoid the adverse effects observed in patients receiving systemic GnRHa therapy.

Author contributions

Conceptualization and work design, C.E., T.A.A. and A.D.; methodology and experimental work, A.S., P.G.G. and P.D.R.; data analyses and interpretation of finding, A.S., P.D.R, T.A.A. and A.D.; writing and review, A.S., P.G.G., P.D.R., C.E., T.A.A. and A.D.; funding acquisition, C.E and A.D. All authors have read and agreed to the published version of

the manuscript.

Conflict of interest statement

The authors declare no conflict of interest.

Acknowledgements

This work is part of the project RTI2018–097324-B-I00 funded by MCIN/AEI/ 10.13039/501100011033 and by "ERDF A way of making Europe". Ana Salas and Patricia García-García acknowledge the University of La Laguna for their fellowship grants (Contratos predoctorales "Cajasiete" para la formación de doctores and contratos predoctorales M-ULL para la formación de doctores, respectively).

Appendix A. Supporting information

Supplementary data associated with this article can be found in the online version at doi:10.1016/j.biopha.2022.113909.

References

[1] E.A. Stewart, Clinical practice. Uterine fibroids, The, N. Engl. J. Med. 372 (17) (2015) 1646–1655.
[2] E. Giuliani, S. As-Sanie, E.E. Marsh, Epidemiology and management of uterine fibroids, Int. J. Gynaecol. Obstet.: Off. Organ Int. Fed. Gynaecol. Obstet. 149 (1) (2020) 3–9.
[3] E. Somigliana, M. Reschini, V. Bonanni, A. Busnelli, L. Li Piani, P. Vercellini, Fibroids and natural fertility: a systematic review and meta-analysis, Reprod. Biomed. Online 43 (1) (2021) 100–110.
[4] E.R. Cardozo, A.D. Clark, N.K. Banks, M.B. Henne, B.J. Stegmann, J.H. Segars, The estimated annual cost of uterine leiomyomata in the United States, Am. J. Obstet. Gynecol. 206 (3) (2012), 211 e1-9.
[5] M. Mehine, E. Kaasinen, H.R. Heinonen, N. Makinen, K. Kampjarvi, N. Sarvilinna, M. Aavikko, A. Vaharautio, A. Pasanen, R. Butzow, O. Heikinheimo, J. Sjoberg, E. Pitkanen, P. Vahteristo, L.A. Aaltonen, Integrated data analysis reveals uterine leiomyoma subtypes with distinct driver pathways and biomarkers, Proc. Natl. Acad. Sci. USA 113 (5) (2016) 1315–1320.
[6] T.D. Lewis, M. Malik, J. Britten, A.M. San Pablo, W.H. Catherino, A. Comprehensive, Review of the pharmacologic management of uterine leiomyoma, BioMed. Res. Int. 2018 (2018) 2414609.
[7] D. Heber, R. Dodson, R.S. Swerdloff, K. Channabasavaiah, J.M. Stewart, Pituitary receptor site blockade by a gonadotropin-releasing hormone antagonist in vivo: mechanism of action, Science 216 (4544) (1982) 420–421.
[8] M.S. Islam, A. Ciavattini, F. Petraglia, M. Castellucci, P. Ciarmela, Extracellular matrix in uterine leiomyoma pathogenesis: a potential target for future therapeutics, Hum. Reprod. Update 24 (1) (2018) 59–85.
[9] A. Al-Hendy, L. Bradley, C.D. Owens, H. Wang, K.T. Barnhart, E. Feinberg, W. D. Schlaff, E.E. Puscheck, A. Wang, V. Gillispie, S. Hurtado, O. Muneyyirci-Delale, D.F. Archer, B.R. Carr, J.A. Simon, E.A. Stewart, Predictors of response for elagolix with add-back therapy in women with heavy menstrual bleeding associated with uterine fibroids, Am. J. Obstet. Gynecol. 224 (1) (2021) 72, e1-72 e50.
[10] A. Al-Hendy, A.S. Lukes, A.N. Poindexter 3rd, R. Venturella, C. Villarroel, H.O. D. Critchley, Y. Li, L. McKain, J.C. Arjona Ferreira, A.G.M. Langenberg, R. B. Wagman, E.A. Stewart, Treatment of uterine fibroid symptoms with relugolix combination therapy, N. Engl. J. Med. 384 (7) (2021) 630–642.
[11] D. Heber, J.C. Marshall, W.D. Odell, GnRH membrane binding: identification, specificity, and quantification in nonpituitary tissues, Am. J. Physiol. 235 (2) (1978) E227–E230.
[12] P. Limonta, R.M. Moretti, M. Montagnani Marelli, M. Motta, The biology of gonadotropin hormone-releasing hormone: role in the control of tumor growth and progression in humans, Front. Neuroendocrinol. 24 (4) (2003) 279–295.
[13] H.M. Wu, H.S. Wang, H.Y. Huang, Y.K. Soong, C.D. MacCalman, P.C. Leung, GnRH signaling in intrauterine tissues, Reproduction 137 (5) (2009) 769–777.
[14] A. Wiznitzer, M. Marbach, E. Hazum, V. Insler, Y. Sharoni, J. Levy, Gonadotropin-releasing hormone specific binding sites in uterine leiomyomata, Biochem. Biophys. Res. Commun. 152 (3) (1988) 1326–1331.
[15] N. Chegini, H. Rong, Q. Dou, S. Kipersztok, R.S. Williams, Gonadotropin-releasing hormone (GnRH) and GnRH receptor gene expression in human myometrium and leiomyomata and the direct action of GnRH analogs on myometrial smooth muscle cells and interaction with ovarian steroids in vitro, The, J. Clin. Endocrinol. Metab. 81 (9) (1996) 3215–3221.
[16] Y. Kobayashi, Y.L. Zhai, M. Iinuma, A. Horiuchi, T. Nikaido, S. Fujii, Effects of a GnRH analogue on human smooth muscle cells cultured from normal myometrial and from uterine leiomyomal tissues, Mol. Hum. Reprod. 3 (2) (1997) 91–99.
[17] Y. Wang, H. Matsuo, O. Kurachi, T. Maruo, Down-regulation of proliferation and up-regulation of apoptosis by gonadotropin-releasing hormone agonist in cultured uterine leiomyoma cells, Eur. J. Endocrinol. 146 (3) (2002) 447–456.
[18] J.D. Parker, M. Malik, W.H. Catherino, Human myometrium and leiomyomas express gonadotropin-releasing hormone 2 and gonadotropin-releasing hormone 2 receptor, Fertil. Steril. 88 (1) (2007) 39–46.
[19] D. Plewka, J. Marczynski, M. Morek, E. Bogunia, A. Plewka, Receptors of hypothalamic-pituitary-ovarian-axis hormone in uterine myomas, BioMed. Res. Int. 2014 (2014), 521313.
[20] W. Chen, S. Yoshida, N. Ohara, H. Matsuo, M. Morizane, T. Maruo, Gonadotropin-releasing hormone antagonist cetrorelix down-regulates proliferating cell nuclear antigen and epidermal growth factor expression and up-regulates apoptosis in association with enhanced poly(adenosine 5′-diphosphate-ribose) polymerase expression in cultured human leiomyoma cells, J. Clin. Endocrinol. Metab. 90 (2) (2005) 884–892.
[21] J.L. Britten, M. Malik, G. Levy, M. Mendoza, W.H. Catherino, Gonadotropin-releasing hormone (GnRH) agonist leuprolide acetate and GnRH antagonist cetrorelix acetate directly inhibit leiomyoma extracellular matrix production, Fertil. Steril. 98 (5) (2012) 1299–1307.
[22] Y. Imamura, T. Mukohara, Y. Shimono, Y. Funakoshi, N. Chayahara, M. Toyoda, N. Kiyota, S. Takao, S. Kono, T. Nakatsura, H. Minami, Comparison of 2D- and 3D-culture models as drug-testing platforms in breast cancer, Oncol. Rep. 33 (4) (2015) 1837–1843.
[23] M. Malik, J. Britten, J. Cox, A. Patel, W.H. Catherino, Gonadotropin-releasing hormone analogues inhibit leiomyoma extracellular matrix despite presence of gonadal hormones, Fertil. Steril. 105 (1) (2016) 214–224.
[24] P.S. Gillies, D. Faulds, J.A. Balfour, C.M. Perry, Ganirelix, Drugs 59(1) (2000) 107–11; discussion 112–3.
[25] P.A. Flierman, J.J. Oberye, V.P. van der Hulst, S. de Blok, Rapid reduction of leiomyoma volume during treatment with the GnRH antagonist ganirelix, BJOG: Int. J. Obstet. Gynaecol. 112 (5) (2005) 638–642.
[26] B. Singh, H. Sims, I. Trueheart, K. Simpson, K.C. Wang, K. Patzkowsky, T. Wegman, J.M. Soma, R. Dixon, F. Jayes, K. Voegltine, G. Yenokyan, S.C. Su, P. Leppert, J. H. Segars, A. Phase, I. Clinical, Trial to assess safety and tolerability of injectable collagenase in women with symptomatic uterine fibroids, Reprod. Sci. 28 (9) (2021) 2699–2709.
[27] A. Salas, J. Lopez, R. Reyes, C. Evora, F.M. de Oca, D. Baez, A. Delgado, T. A. Almeida, Organotypic culture as a research and preclinical model to study uterine leiomyomas, Sci. Rep. 10 (1) (2020) 5212.
[28] P. Garcia-Garcia, R. Reyes, E. Perez-Herrero, M.R. Arnau, C. Evora, A. Delgado, Alginate-hydrogel versus alginate-solid system. Efficacy in bone regeneration in osteoporosis, Materials science & engineering, C., Mater. Biol. Appl. 115 (2020), 111009.
[29] G. Gainza, J.J. Aguirre, J.L. Pedraz, R.M. Hernandez, M. Igartua, rhEGF-loaded PLGA-Alginate microspheres enhance the healing of full-thickness excisional wounds in diabetised Wistar rats, Eur. J. Pharm. Sci.: Off. J. Eur. Fed. Pharm. Sci. 50 (3–4) (2013) 243–252.
[30] P. Zhai, X.B. Chen, D.J. Schreyer, PLGA/alginate composite microspheres for hydrophilic protein delivery, Materials science & engineering, C., Mater. Biol. Appl. 56 (2015) 251–259.
[31] J. Zhai, Y.E. Wang, X. Zhou, Y. Ma, S. Guan, Long-term sustained release Poly (lactic-co-glycolic acid) microspheres of asenapine maleate with improved bioavailability for chronic neuropsychiatric diseases, Drug Deliv. 27 (1) (2020) 1283–1291.
[32] C. Del Rosario, M. Rodriguez-Evora, R. Reyes, A. Delgado, C. Evora, BMP-2, PDGF-BB, and bone marrow mesenchymal cells in a macroporous beta-TCP scaffold for critical-size bone defect repair in rats, Biomed. Mater. 10 (4) (2015), 045008.
[33] B. De la Riva, C. Nowak, E. Sanchez, A. Hernandez, M. Schulz-Siegmund, M.K. Pec, A. Delgado, C. Evora, VEGF-controlled release within a bone defect from alginate/chitosan/PLA-H scaffolds, Eur. J. Pharm. Biopharm.: Off. J. Arb. fur Pharm. Verfahr. e. V. 73 (1) (2009) 50–58.
[34] L. Merz, S. Hobel, S. Kallendrusch, A. Ewe, I. Bechmann, H. Franke, F. Merz, A. Aigner, Tumor tissue slice cultures as a platform for analyzing tissue-penetration and biological activities of nanoparticles, Eur. J. Pharm. Biopharm.: Off. J. Arb. fur Pharm. Verfahr. e. V. 112 (2017) 45–50.
[35] K. Tamura, G. Stecher, D. Peterson, A. Filipski, S. Kumar, MEGA6: molecular evolutionary genetics analysis version 6.0, Mol. Biol. Evol. 30 (12) (2013) 2725–2729.
[36] T.A. Almeida, A. Quispe-Ricalde, F. Montes de Oca, P. Foronda, M.M. Hernandez, A high-throughput open-array qPCR gene panel to identify housekeeping genes suitable for myometrium and leiomyoma expression analysis, Gynecol. Oncol. 134 (1) (2014) 138–143.
[37] J.A. Kiernan, Histological and histochemical methods: Theory and practice, Banbury, UK, 2015.
[38] R. de Hoogt, M.F. Estrada, S. Vidic, E.J. Davies, A. Osswald, M. Barbier, V.E. Santo, K. Gjerde, H. van Zoggel, S. Blom, M. Dong, K. Narhi, E. Boghaert, C. Brito, Y. Chong, W. Sommergruber, H. van der Kuip, W.M. van Weerden, E. W. Verschuren, J. Hickman, R. Graeser, Protocols and characterization data for 2D, 3D, and slice-based tumor models from the PREDECT project, Sci. data 4 (2017), 170170.
[39] E.J. Davies, M. Dong, M. Gutekunst, K. Narhi, H.J. van Zoggel, S. Blom, A. Nagaraj, T. Metsalu, E. Oswald, S. Erkens-Schulze, J.A. Delgado San Martin, R. Turkki, S. R. Wedge, T.M. af Hallstrom, J. Schueler, W.M. van Weerden, E.W. Verschuren, S. T. Barry, H. van der Kuip, J.A. Hickman, , Capturing Complex Tumour Biol. Vitr.: Histol. Mol. Character Precis. Cut. slices, Sci. Rep. 5 (2015) 17187.
[40] S. Huerta, E.J. Goulet, S. Huerta-Yepez, E.H. Livingston, Screening and detection of apoptosis, The, J. Surg. Res. 139 (1) (2007) 143–156.
[41] N. Wilkinson, T.P. Rollason, Recent advances in the pathology of smooth muscle tumours of the uterus, Histopathology 39 (4) (2001) 331–341.

[42] V. Vaira, G. Fedele, S. Pyne, E. Fasoli, G. Zadra, D. Bailey, E. Snyder, A. Faversani, G. Coggi, R. Flavin, S. Bosari, M. Loda, Preclinical model of organotypic culture for pharmacodynamic profiling of human tumors, Proc. Natl. Acad. Sci. USA 107 (18) (2010) 8352–8356.
[43] K.A. Naipal, N.S. Verkaik, H. Sanchez, C.H. van Deurzen, M.A. den Bakker, J. H. Hoeijmakers, R. Kanaar, M.P. Vreeswijk, A. Jager, D.C. van Gent, Tumor slice culture system to assess drug response of primary breast cancer, BMC Cancer 16 (2016) 78.
[44] C.Y. Lim, J.H. Chang, W.S. Lee, K.M. Lee, Y.C. Yoon, J. Kim, I.Y. Park, Organotypic slice cultures of pancreatic ductal adenocarcinoma preserve the tumor microenvironment and provide a platform for drug response, Pancreatol.: Off. J. Int. Assoc. Pancreatol. 18 (8) (2018) 913–927.
[45] O. Tredan, C.M. Galmarini, K. Patel, I.F. Tannock, Drug resistance and the solid tumor microenvironment, J. Natl. Cancer Inst. 99 (19) (2007) 1441–1454.
[46] J. Oberye, B. Mannaerts, J. Huisman, C. Timmer, Local tolerance, pharmacokinetics, and dynamics of ganirelix (Orgalutran) administration by Medi-Jector compared to conventional needle injections, Hum. Reprod. 15 (2) (2000) 245–249.
[47] Y. Su, B. Zhang, R. Sun, W. Liu, Q. Zhu, X. Zhang, R. Wang, C. Chen, PLGA-based biodegradable microspheres in drug delivery: recent advances in research and application, Drug Deliv. 28 (1) (2021) 1397–1418.
[48] P. Limonta, M. Montagnani Marelli, S. Mai, M. Motta, L. Martini, R.M. Moretti, GnRH receptors in cancer: from cell biology to novel targeted therapeutic strategies, Endocr. Rev. 33 (5) (2012) 784–811.
[49] N.A. Ciccone, U.B. Kaiser, The biology of gonadotroph regulation, Current opinion in endocrinology, Diabetes, Obes. 16 (4) (2009) 321–327.
[50] A. Imai, H. Takagi, T. Furui, S. Horibe, T. Fuseya, T. Tamaya, Evidence for coupling of phosphotyrosine phosphatase to gonadotropin-releasing hormone receptor in ovarian carcinoma membrane, Cancer 77 (1) (1996) 132–137.
[51] A.V. Schally, A.M. Comaru-Schally, A. Nagy, M. Kovacs, K. Szepeshazi, A. Plonowski, J.L. Varga, G. Halmos, Hypothalamic hormones and cancer, Front. Neuroendocrinol. 22 (4) (2001) 248–291.
[52] S. Maudsley, L. Davidson, A.J. Pawson, R. Chan, R. Lopez de Maturana, R.P. Millar, Gonadotropin-releasing hormone (GnRH) antagonists promote proapoptotic signaling in peripheral reproductive tumor cells by activating a Galphai-coupling state of the type I GnRH receptor, Cancer Res. 64 (20) (2004) 7533–7544.
[53] C. Grundker, G. Emons, The role of gonadotropin-releasing hormone in cancer cell proliferation and metastasis, Front. Endocrinol. 8 (2017) 187.
[54] J.A. Halterman, H.M. Kwon, B.R. Wamhoff, Tonicity-independent regulation of the osmosensitive transcription factor TonEBP (NFAT5), Am. J. Physiol. Cell Physiol. 302 (1) (2012) C1–C8.
[55] D.M. McCarthy-Keith, M. Malik, J. Britten, J. Segars, W.H. Catherino, Gonadotropin-releasing hormone agonist increases expression of osmotic response genes in leiomyoma cells, Fertil. Steril. 95 (7) (2011) 2383–2387.
[56] J.L. Britten, M. Malik, T.D. Lewis, W.H. Catherino, Ulipristal acetate mediates decreased proteoglycan expression through regulation of nuclear factor of activated T-cells (NFAT5), Reprod. Sci. 26 (2) (2019) 184–197.